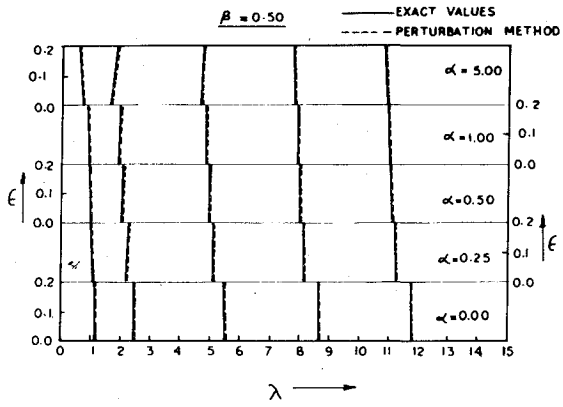

Fig. 4 Comparison of natural frequencies by perturbation method with exact values, $\beta = 0.50$.

where L is the length of the beam, and ℓ is the distance between point of attachment and the center of gravity of the tip mass. For free harmonic vibrations with frequency ω, the exact frequency equation is obtained as

$$1 + \alpha\beta\lambda^4 + (1-\alpha\beta\lambda^4)G(\lambda) + \alpha\lambda[H(\lambda) - J(\lambda)] - \beta\lambda^3[H(\lambda) + J(\lambda)] - 2\alpha\epsilon\lambda^2 F(\lambda) - \alpha\epsilon^2\lambda^3[H(\lambda) + J(\lambda)] = 0 \quad (4)$$

where

$$F(\lambda) = \sinh\lambda \cdot \sin\lambda, \quad G(\lambda) = \cosh\lambda \cdot \cos\lambda,$$
$$H(\lambda) = \sinh\lambda \cdot \cos\lambda, \quad J(\lambda) = \cosh\lambda \cdot \sin\lambda$$

and

$$\lambda^4 = m\omega^2 L^4/EI, \quad \alpha = M/mL, \quad \epsilon = \ell/L, \quad \beta = J_0/mL^3.$$

The solution of the frequency equation given by Eq. (4), for small values of ϵ, was obtained by a perturbation procedure,[5] where the frequencies can be obtained as

$$\lambda = \lambda_0 + \epsilon\lambda_1 + \epsilon^2\lambda_2 + \ldots\ldots \quad (5)$$

where

$$\lambda_1 = 2\alpha\lambda_0^2 F(\lambda_0)/\{4\beta\lambda_0^3[1-G(\lambda_0)] + \alpha(1-\beta\lambda_0^4) \times [H(\lambda_0) - J(\lambda_0)] - 2\alpha\lambda_0 F(\lambda_0) - 2\beta\lambda_0^3 G(\lambda_0) - 3\beta\lambda_0^2[H(\lambda_0) + J(\lambda_0)]\} \quad (6)$$

and

$$\lambda_2 = \{(4\alpha\lambda_0\lambda_1 + 2\alpha\lambda_1^2 - \alpha\beta\lambda_0^4\lambda_1^2)F(\lambda_0) + (\beta\lambda_0^3\lambda_1^2 + 4\alpha\beta\lambda_0^3\lambda_1^2)[H(\lambda_0) - J(\lambda_0)] + 6\beta\lambda_0^2\lambda_1^2 G(\lambda_0) + (\lambda_0\lambda_1^2 + 3\beta\lambda_0\lambda_1^2 - 2\alpha\lambda_0^2\lambda_1 + \alpha\lambda_0^3)[H(\lambda_0) + J(\lambda_0)] - 6\alpha\beta\lambda_0^2\lambda_1^2[1-G(\lambda_0)]\}/\{4\alpha\beta\lambda_0^3[1-G(\lambda_0)] + \alpha(1-\beta\lambda_0^4)[H(\lambda_0) - J(\lambda_0)] - 2\lambda_0 F(\lambda_0) - 3\beta\lambda_0^2[H(\lambda_0) + J(\lambda_0)] - 2\beta\lambda_0^3 G(\lambda_0)\} \quad (7)$$

The exact values of the natural frequencies for the first five modes, obtained by solving Eq. (4) in a digital computer, are compared with those obtained by the perturbation method, for various values of ϵ, in Figs. 2-4. It can be seen that, except in Fig. 2 for the case of $\beta = 0.0$, the perturbation method gives good results. Every mass will have reasonable moment of inertia, i.e., β will not be zero in practical cases. Hence, the perturbation method can be used to get natural frequencies with good accuracy.

References

[1] Pipes, L.A., *Applied Mathematics for Engineers and Physicists*, McGraw-Hill, New York, 1958, pp. 536-539.

[2] Prescott, J., *Applied Elasticity*, Dover, New York, 1946, pp. 213-218.

[3] Temple, G. and Bickley, W.G., "Rayleigh's Principal," Dover, New York, 1956, pp. 110-112.

[4] Durvasula, S., "Vibrations of Uniform Cantilever Beam Carrying a Concentrated Mass and Moment of Inertia at the Tip," AE 1338, 1965, Dept. of Aeronautical Engineering, Indian Institute of Science, Bangalore, India.

[5] Rama Bhat, B. and Wagner, H., "Natural Frequencies of a Uniform Cantilever with a Tip Mass Slender in the Axial Direction," *Journal of Sound and Vibration*, Vol. 44, 1976, (to be published).

Shock Detachment Distance at Near Sonic Speeds

R.F. Starr,* A.B. Bailey,† and M.O. Varner‡
ARO, Inc., Arnold Air Force Station, Tenn.

THIS Note documents some recent experimental observations of the shock detachment distance for spherical and spherically blunted bodies at near-sonic speeds ($1.0 < M_\infty < 1.5$) in air. Spheres and spherically blunted cones have been tested in the 10-ft-diam AEDC Aeroballistic Range G to determine their transonic drag characteristics. The bow shock ahead of the body is clearly visible in shadowgraph pictures taken of the model in flight which are used to establish the time-distance relationship and drag. A sequence of photographs illustrating the variation of shock detachment distance with Mach number for the sphere is shown in Fig. 1. This 1.5-in.-diam sphere was tested at a solid blockage of 0.016% which is considered to be interference free. The Reynolds number based on diameter, Re_d for this study was approximately 1×10^6. A sequence of photographs of the shock detachment variation with Mach number for a 10° semiangle, 0.3 bluntness ratio, d_n/d, cone is displayed in Fig. 2. This 3-in. base-diam cone was tested at a solid blockage based on the model base diameter d of 0.0625%. The Re_d was approximately 2×10^6 for these tests. The results presented herein are free of the influence of (1) the blast wave which emanates from the muzzle of the model launcher, and (2) deceleration of the model during flight. Both of these problems can be encountered in testing in aeroballistic ranges at speeds very near Mach 1 and involving rapid decelerations. The presence of a blast wave just ahead of a model results in an induced velocity field and a reduced effective Mach number. Rapid deceleration of the model results in a mislocation of the shock for any instantaneous Mach number, since a finite flow response time is invloved. Such effects were avoided in the present study by careful selection of model mass and launch velocity.

Received Dec. 8, 1975, The research reported herein was conducted by the Arnold Engineering Development Center (AEDC), Air Force Systems Command (AFSC), U.S. Air Force. Research results were obtained by personnel of ARO, Inc., contract operator of AEDC. Further reproduction is authorized to satisfy needs of the U.S. Government.

Index categories: Subsonic and Transonic Flow; Supersonic and Hypersonic Flow.

*Senior Engineer. Member AIAA.
†Research Engineer. Associate Fellow AIAA.
‡Research Engineer. Member AIAA.

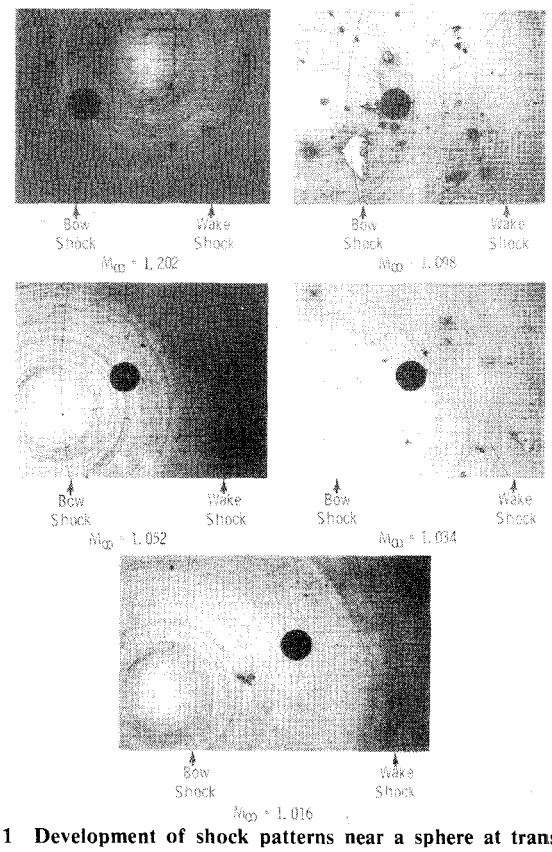

Fig. 1 Development of shock patterns near a sphere at transonic speeds.

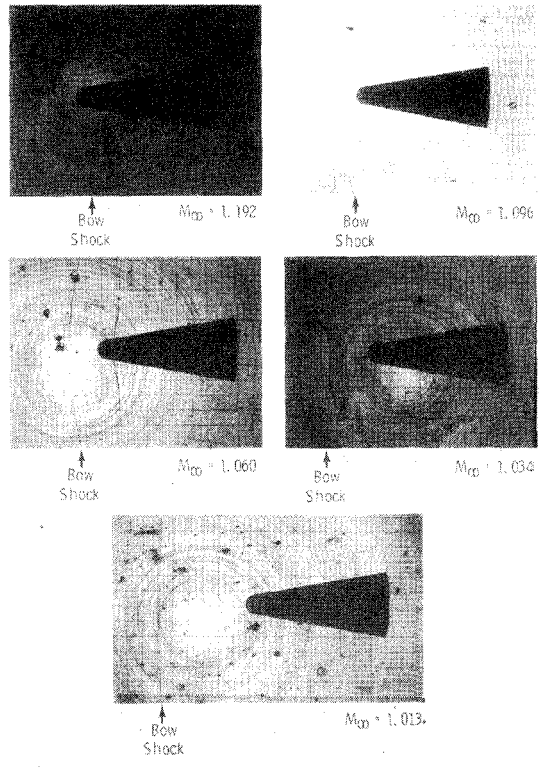

Fig. 2 Development of shock patterns near a cone at transonic speeds.

The variation of shock detachment distance for $1.0 \leq M_\infty \leq 1.2$ is given in Fig. 3a for the spheres and several blunted cones. The very rapid increase in shock detachment distance is evident at Mach numbers below 1.1. Two important observations can be made based on the data in Fig. 3a. First, the

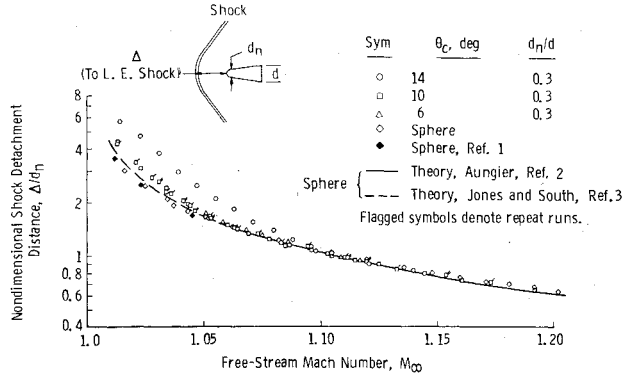

Fig.3a Shock detachment distance vs Mach number for spheres and spherically blunted cones at transonic speeds.

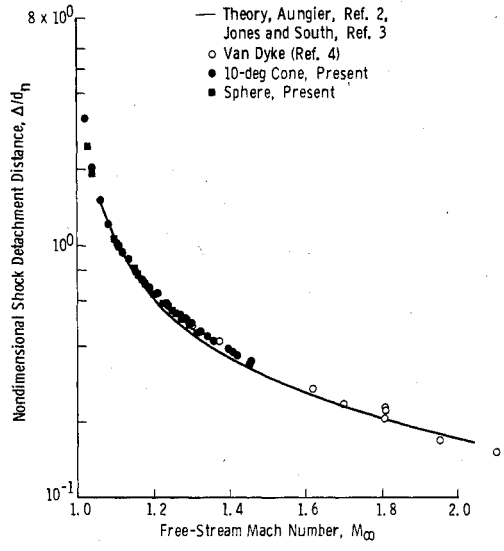

Fig. 3b Shock detachment distance vs Mach number for spheres and spherically blunted cones in the transonic and low supersonic Regime.

repeatability of this very sensitive parameter with Mach number is excellent, as shown by the agreement of the three different 0.3 bluntness, 10°semiangle cone shots in the 1.01 - 1.15 Mach number range. Second, the shock detachment distance is not a simple function of the body nose diameter as $M_\infty \to 1$, since the location of the sonic line can move past the intersection of the spherical nose and the conical afterbody. The shock detachment distance then becomes a function of the local geometry of the afterbody at the sonic line location. This is illustrated by the fact that the sphere, the 10°, and the 14° semiangle cone data disgress slightly as the Mach number approaches 1.0. Data obtained on a 0.25-in.-diam sphere[1] in a 6-ft-diam range, solid blockage of 0.0012%, at a $Re_d \approx 10^3$ (which ensures laminar continuum flow) also are shown in Fig. 3a. Existing theoretical flowfield solutions for spheres by Aungier[2] and Jones and South[3] presented in Fig. 3a are in good agreement with the experimental measurements. Additional results from the present study at Mach numbers up to 1.5 are presented in Fig. 3b, along with typical previous results[4] and the theoretical solutions.

References

[1] Bailey, A.B. and Hiatt, J., "Free-Flight Measurements of Sphere Drag at Subsonic, Transonic, Supersonic, and Hypersonic Speeds for Continuum, Transition, and Near-Free-Molecular Flow Conditions," AEDC-TR-70-291 (AD721208), March 1971, Arnold Engineering Development Center, Arnold Air Force Station, Tenn.

[2] Aungier, R.H.., "A Computational Method for Exact, Direct, and Unified Solutions for Axisymmetric Flow Over Blunt Bodies of Ar-

bitrary Shape (Program BLUNT)," AFWL-TR-70-16, July 1970 Air Force Weapons Lab. Kirtland AFB, New Mex.

[3] Jones, D.J. and South, J.C., Jr., "A Numerical Determination of the Bow Shock Wave in Transonic Axisymmetric Flow About Blunt Bodies," NAE LR-586, May 1975, National Research Council, Ottawa, Canada.

[4] Van Dyke, M.D. and Gordon, H.D. "Supersonic Flow Past a Family of Blunt Axisymmetric Bodies," TR R-1, Oct. 1958, NASA.

Comparison of a Two-Dimensional Shock Impingement Computation with Experiment

J.C. Tannehill* and T.L. Holst†
Iowa State University, Ames, Iowa
J.V. Rakich‡
NASA Ames Research Center, Moffett Field, Calif.
and
J.W. Keyes§
NASA Langley Research Center, Hampton, Va.

Nomenclature

C = smoothing constant
M = Mach number
p = pressure
Pr = Prandtl number
q = heat flux
Re_D = Reynolds number based on diameter
T = temperature
β = stretching factor
γ = specific heat ratio
θ = angle measured from stagnation streamline (without impingement)

Subscripts

stag = stagnation point value (without impingement)
w = wall value
∞ = freestream value

In Ref. 1, two-dimensional, viscous, blunt-body flowfields with an impinging shock wave were computed using a time-dependent, finite-difference method to solve the complete set of Navier-Stokes equations. These computations were qualitatively compared with existing three-dimensional experiments because of the lack of suitable two-dimensional experiments. Recently, J.W. Keyes completed a series of two-dimensional tests in the Langley 20-in. Hypersonic Tunnel. In these tests, a planar shock wave was allowed to impinge on the cylindrical leading edge of a fin (shock parallel with centerline of leading edge) resulting in Type III and Type IV interference patterns.[2] The computational method described in Ref. 1 was used to compute numerically one of the Type IV flowfields. This Note compares the results of this computation with the experiment. In addition, recent numerical experiments showing the effects of grid size and numerical smoothing are presented to better establish the accuracy of the code.

Received November 3, 1975; revision received January 5, 1976. The computational work in this paper was supported by NASA Ames Research Center under Grant NGR 16-002-038 and the Engineering Research Institute, Iowa State University, Ames, Iowa.

Index category: Supersonic and Hypersonic Flow.

*Associate Professor, Department of Aerospace Engineering and Engineering Research Institute. Member AIAA.

†Research Associate, Department of Aerospace Engineering and Engineering Research Institute; now Aerospace Engineer, Analytical Fluid Mechanics Section, High-Speed Aerodynamics Division, NASA Langley Research Center. Member AIAA.

‡Research Scientist. Associate Fellow AIAA.

§Aerospace Engineer, Applied Fluid Mechanics Section, High-Speed Aerodynamics Division.

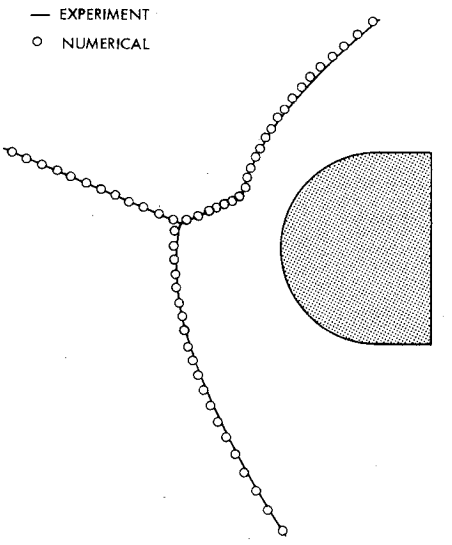

Fig. 1 Comparison of shock shapes.

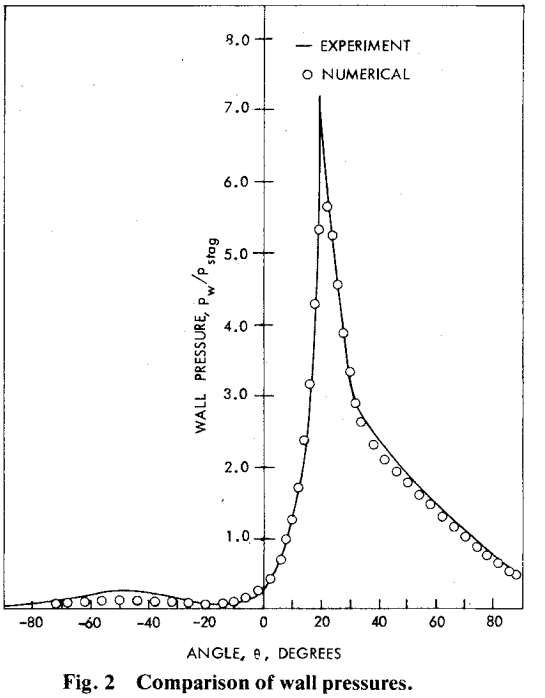

Fig. 2 Comparison of wall pressures.

The conditions of the test case were $M_\infty = 5.94$, $Re_{D_\infty} = 186{,}000$, $Pr = 0.72$, $p_\infty = 536$ N/m^2, $T_\infty = 59.5$ K, and $\gamma = 1.4$ with a leading edge radius of 0.0127 m and a wall temperature of 408 K. The impinging shock was inclined to the freestream at an angle of 22.75° and intersected the bow shock at $\theta = 7°$. Because of the much higher Reynolds number in this case, as compared to the Reynolds number in the cases of Ref. 1, it was necessary to use substantially more grid points. A grid composed of 81 points around the body ($\theta = -72°$ to $\theta = 88°$) and 61 points normal to it was employed in the final numerical computation. The mesh was refined near the body using a stretching factor (β) equal to 1.025. For this value of β, the first grid point off the body is located at 0.19% of the shock standoff distance as compared with 1.67% for no stretching.

A comparison between the numerical and experimental shock shapes is shown in Fig. 1. Excellent agreement is achieved. A comparison between the numerical and experimental wall pressures is shown in Fig. 2. Again, the com-